



OPEN ACCESS

EDITED BY

Hu Li,
Guizhou University, China

REVIEWED BY

P. Kamaraj,
Bharath Institute of Science and Technology,
India
Qiuyun Zhang,
Anshun University, China

*CORRESPONDENCE

Amar Djemoui,
✉ a.djemoui@univ-djelfa.dz
Ahmed Barhoum,
✉ ahmed.barhoum@science.helwan.edu.eg

RECEIVED 22 November 2023

ACCEPTED 20 December 2023

PUBLISHED 16 January 2024

CITATION

Abdelbaki H, Djemoui A, Souli L, Souadia A, Ouahrani MR, Djemoui B, Lahrech MB, Messaoudi M, Ben Amor I, Benarfa A, Alsalmé A, Bechelany M and Barhoum A (2024), Plant mediated synthesis of flower-like Cu₂O microbeads from *Artimisia campestris* L. extract for the catalyzed synthesis of 1,4-disubstituted 1,2,3-triazole derivatives.
Front. Chem. 11:1342988.
doi: 10.3389/fchem.2023.1342988

COPYRIGHT

© 2024 Abdelbaki, Djemoui, Souli, Souadia, Ouahrani, Djemoui, Lahrech, Messaoudi, Ben Amor, Benarfa, Alsalmé, Bechelany and Barhoum. This is an open-access article distributed under the terms of the [Creative Commons Attribution License \(CC BY\)](https://creativecommons.org/licenses/by/4.0/). The use, distribution or reproduction in other forums is permitted, provided the original author(s) and the copyright owner(s) are credited and that the original publication in this journal is cited, in accordance with accepted academic practice. No use, distribution or reproduction is permitted which does not comply with these terms.

Plant mediated synthesis of flower-like Cu₂O microbeads from *Artimisia campestris* L. extract for the catalyzed synthesis of 1,4-disubstituted 1,2,3-triazole derivatives

Halla Abdelbaki^{1,2}, Amar Djemoui^{3*}, Lahcene Souli³,
Ahmed Souadia⁴, Mohammed Ridha Ouahrani^{1,2},
Brahim Djemoui⁵, Mokhtar Boualem Lahrech³,
Mohammed Messaoudi⁶, Ilham Ben Amor⁷, Adel Benarfa^{8,9},
Ali Alsalmé¹⁰, Mikhael Bechelany^{11,12} and Ahmed Barhoum^{13*}

¹Department of Chemistry, Faculty of Exact Sciences, University of El Oued, El Oued, Algeria, ²Laboratory of Biodiversity and Application of Biotechnology in the Agricultural Field, Faculty of Natural Sciences and Life, University of El Oued, El Oued, Algeria, ³Laboratory of Organic Chemistry and Natural Substance, Department of Chemistry, Faculty of Exact Sciences and Computer Science, ZIANE Achour University, Djelfa, Algeria, ⁴Laboratory of Physico-Chemistry of Materials and Environment, Department of Chemistry, Faculty of Exact Sciences and Computer Science, ZIANE Achour University, Djelfa, Algeria, ⁵Department of Chemistry, Faculty of Exact and Applied Sciences (FSEA), Oran University1, Oran, Algeria, ⁶Nuclear Research Centre of Birine (CRNB), Djelfa, Algeria, ⁷Department of Process Engineering and Petrochemical, Faculty of Technology, University of El Oued, El Oued, Algeria, ⁸Laboratoire des Sciences Fondamentales (LSF), University of Amar Têlidji Laghouat, Laghouat, Algeria, ⁹Centre de Recherche Scientifique et Technique en Analyses Physico-Chimiques (CRAPC)-PTAPC, Laghouat, Algeria, ¹⁰Department of Chemistry, College of Science, King Saud University, Riyadh, Saudi Arabia, ¹¹Institut Européen des Membranes (IEM), UMR 5635, University Montpellier, ENSCM, CNRS, Place Eugène Bataillon, Montpellier, France, ¹²Gulf University for Science and Technology, GUST, Mubarak Al-Abdullah, Kuwait, ¹³NanoStruc Research Group, Chemistry Department, Faculty of Science, Helwan University, Cairo, Egypt

This study presents a novel method for synthesizing 1,4-disubstituted 1,2,3-triazole derivatives through a one-pot, multi-component addition reaction using flower-like Cu₂O microbeads as a catalyst. The flower-like Cu₂O microbeads were synthesized using an aqueous extract of *Artimisia Campestris* L. This extract demonstrated the capability to reduce and stabilize Cu₂O particles during their initial formation, resulting in the formation of a porous flower-like morphology. These Cu₂O microbeads exhibit distinctive features, including a cubic close-packed (ccp) crystal structure with an average crystallite size of 22.8 nm, bandgap energy of 2.7 eV and a particle size of 6 μm. Their catalytic activity in synthesizing 1,4-disubstituted 1,2,3-triazole derivatives was investigated through systematic exploration of key parameters such as catalyst quantity (1, 5, 10, 15, 20, and 30 mg/mL), solvent type (dimethylformamide/H₂O, ethanol/H₂O, dichloromethane/H₂O, chloroform, acetone, and dimethyl sulfoxide), and catalyst reusability (four cycles). The Cu₂O microbeads significantly increased the product yield from 20% to 85.3%. The green

synthesis and outstanding catalytic attributes make these flower-like Cu_2O microbeads promising, efficient, and recyclable catalysts for sustainable and effective chemical transformations.

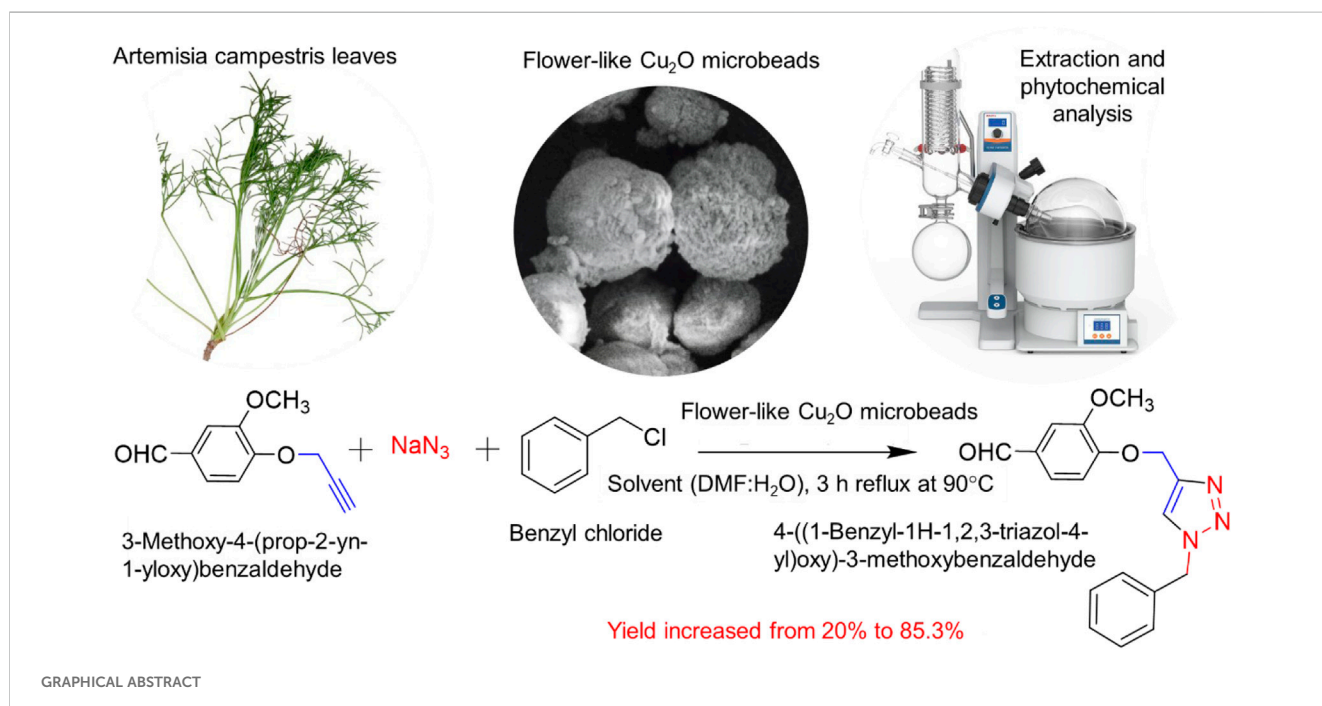
KEYWORDS

cuprous oxide, flower-like nanostructures, *Artimisia Campestris* L. extract, green synthesis, 1,4-disubstituted 1,2,3-triazoles

1 Introduction

1,4-Disubstituted 1,2,3-triazole derivatives are a class of organic compounds characterized by a triazole ring at their core (Kawka et al., 2023). These compounds have multifaceted biological properties and potential therapeutic applications, making them valuable bioactive agents (Parvizi et al., 2019). These compounds exhibit resistance to oxidation, reduction, and hydrolysis under both acidic and basic conditions (De Nino et al., 2018). Copper-based compounds stand as a predominant catalyst employed in synthesis 1,4-disubstituted 1,2,3-triazole due to its affordability and reduced toxicity (Dai et al., 2022). However, the challenge of separating the catalyst from the end product poses economic and environmental obstacles its application (Shaabani et al., 2017). To address this challenge, heterogeneous catalysts using metal-based micro/nanoparticles. These include copper (De Nino et al., 2021), silver (Sultana and Sarma, 2020), zinc (Daraie et al., 2020), ruthenium (Sharma et al., 2018), iridium (Wu et al., 2020), nickel (Choudhury et al., 2021), and gold (Librando et al., 2021) providing alternatives to traditional homogeneous catalysts. The employment of these catalysts allows for straightforward separation from the reaction solution via simple filtration, promoting their reusability (Aronica and Albano, 2022). This approach addresses the limitations associated with catalyst separation, enhancing the sustainability and efficiency of 1,4-disubstituted 1,2,3-triazole synthesis processes.

Cuprous oxide (Cu_2O) has emerged as a versatile and efficient heterogeneous catalyst for a wide range of organic synthesis reactions, offering greener and more sustainable alternatives to traditional methods (Yadav et al., 2019). Cu_2O proves effective in C–H arylation reactions, facilitating the introduction of aryl groups into organic compounds, and it plays a role in carbon-carbon coupling reactions. Its unique properties make it particularly well-suited for catalyzing diverse transformations (click reactions, redox reactions, cross-coupling reactions, hydrolyzation, C–H activation) in organic chemistry (Ojha et al., 2017). For instance, Cu_2O micro/nanoparticles facilitate controlled oxidation, converting alcohols to carbonyl compounds, and is involved in reduction reactions, reducing nitro compounds to amino compounds (Yadav et al., 2019). They have been also employed as catalysts for the copper(I)-catalyzed azide-alkyne cycloaddition (CuAAC) reaction (Varzi et al., 2021), which provides an efficient and eco-friendly route to synthesize 1,2,3-triazole derivatives (Moeini-Eghbali and Eshghi, 2023). This method eliminates the need for toxic and moisture-sensitive reagents often used in traditional approaches, showcasing the green chemistry aspect of Cu_2O catalysis (Moeini-Eghbali and Eshghi, 2023). Another remarkable example is the synthesis of arylamines via the reduction of nitro compounds, and the use of Cu_2O nanoparticles as a catalyst which minimizes the use of hazardous reagents and reduces waste production (Sasmal et al., 2016; Roemer et al., 2022).



Traditionally, Cu₂O micro/nanoparticles have been synthesized using various techniques such as microwave irradiation, vapor deposition, thermal decomposition, and electrochemical methods (Mallik et al., 2020). However, these methods come with some limitations, encompassing challenges related to scalability and purification, substantial energy consumption, and the use of hazardous chemicals (Le et al., 2021). To overcome these challenges, green synthesis methods using plant extracts and microorganisms have been developed for producing Cu₂O particles. Plant extracts are often preferred for their simplicity and rapid reduction capabilities, whereas microorganisms offer versatility and the potential for controlled synthesis under specific conditions (Varghese et al., 2020). Numerous studies have reported successful synthesis of Cu₂O particles using plant extracts, including *banana pulp* waste (Torres-Arellano et al., 2021), *Aloe vera* (Kerour et al., 2018), *Piper longum* (Murphin Kumar et al., 2020), and *Cressa* leaf (Hui et al., 2022) extracts. These methods not only align with sustainable and eco-friendly principles but also contribute to the expansion of green nanotechnology in the production of Cu₂O NPs for diverse applications (Waris et al., 2021).

This study explores the synthesis of flower-like Cu₂O microbeads using an aqueous extract of *Artemisia Campestris L.*, which are subsequently employed as catalysts in the synthesis of 1,4-disubstituted 1,2,3-triazole derivatives. The approach not only leverages natural resources from the *Artemisia Campestris L.* extract, presenting a sustainable and eco-friendly method for producing catalytic Cu₂O microbeads but also demonstrates their application in the synthesis of 1,4-disubstituted 1,2,3-triazole derivatives. Characterization of 1,4-disubstituted 1,2,3-triazole derivatives were performed by thin-layer chromatography (TLC), hydrogen nuclear magnetic resonance (H-NMR), carbon-13 nuclear magnetic resonance (C-NMR), Fourier transform infrared red spectroscopy (FTIR), and for Cu₂O microbeads, X-ray diffraction (XRD), UV-Vis spectroscopy, Infra-Red (FTIR) spectroscopy, and scanning electron microscopy (SEM) are employed. The study extended to discuss the crucial factors to producing 1,4-disubstituted 1,2,3-triazole derivatives such as catalyst quantity, solvent choice, and catalyst reusability. Overall, this research holds significant promise in advancing green chemistry principles and contributing to drug discovery.

2 Experimental section

2.1 Materials

Artemisia Campestris L. leaves were collected from local fields in the region of Messad-Djelfa, Algeria (Latitude: 34.1667, Longitude: 3.5 34° 10'0"North, 3° 30'0"East). 4-hydroxybenzaldehyde (C₇H₆O₂, 98%), benzyl chloride (C₇H₇Cl, 99%), 4-methylbenzyl chloride (C₈H₉Cl, 98%), and chloroform (CHCl₃, 99%) were purchased from Sigma-Aldrich Co (Switzerland). Salicylaldehyde (C₇H₆O₂, 95%), sodium azide (NaN₃, 99.5%), N,N-dimethylformamide (DMF, C₃H₇NO, 99.5%), and dimethyl sulfoxide (DMSO, (CH₃)₂SO, 95%) were purchased from BIOCHEM Chemo pharma Co(Canada). Vaniline (C₈H₈O₃, 98%), propargyl bromide (C₃H₃Br, 98% in toluene), copper sulfate pentahydrate (CuSO₄·5H₂O, 99%), ethanol

(EtOH, C₂H₆O, 99.7%), and dichloromethane (CH₂Cl₂, 99.8%) were purchased from Fluka (Buchs, Switzerland). Acetone (C₃H₆O, 97%) and potassium carbonate (K₂CO₃, 97%) were purchased from VWR Chemicals (Ltd., Debrecen Hungary). All chemicals were of analytical reagent grade and used without further purification.

2.2 Plant-mediated synthesis of Cu₂O microbeads

Fresh leaves of *Artemisia Campestris L.* were meticulously washed with tap water, followed by a drying at room temperature for 15 days. Subsequently, the dried leaves were ground into a fine powder. The extraction process was carried out through the maceration method. Specifically, 10 g of the powdered leaves were dispersed in 100 mL of hot deionized water (100°C) in Erlenmeyer flask for duration at 1 h. The resultant extract was subsequently filtered and stored at a temperature of 4°C for subsequent utilization. About 10 mL of aqueous plant extract mixed with 10 mL a 1 M CuSO₄·5H₂O solution. Subsequently, these two solutions were mixed in a suitable ratio under magnetic stirring for 30 min at 70 °C. During the reaction, the initial blue color, attributed to the presence of Cu²⁺ ions, transformed into a persistent reddish-brown suspension, signifying the formation of Cu₂O microbeads as a dispersed phase. The Cu₂O microbeads were then collected through a centrifugation process, and the resultant particles were dried in an electric oven at 80 °C for duration of 2 h to obtain the Cu₂O powder sample.

2.3 Synthesis of 1,4-disubstituted 1,2,3-triazoles

The synthesis of 1,4-disubstituted 1,2,3-triazoles from alkynes (4-(prop-2-yn-1-yloxy) benzaldehyde, 3-methoxy-4-(prop-2-yn-1-yloxy) benzaldehyde, and 1-methoxy-2-(prop-2-yn-1-yloxy) benzene) involves a multistep process outlined in Figure 1. The initial steps focus on the preparation of alkynes derived from various benzaldehyde derivatives, namely, 4-hydroxybenzaldehyde, Vaniline, and Salicylaldehyde (Figures 1A–C) (Tehrani et al., 2019). Anhydrous potassium carbonate (2.5 mmol) was added to a solution of benzaldehyde derivatives (1.0 mmol) in dimethylformamide (DMF), and the resulting mixture was subjected to reflux for 5 min. Subsequently, propargyl bromide (80% in toluene, 1.3 mmol) was added dropwise, and the reaction mixture was stirred for 2 h. The progression of the reaction was monitored using thin-layer chromatography (TLC). Upon completion of the reaction, ice-cold water was introduced to the reaction mixture. The resulting residue was filtered, washed repeatedly with water, and then subjected to recrystallization from ethanol.

For the synthesis of 1,4-disubstituted 1,2,3-triazoles, a reaction was carried out involving benzyl chloride derivatives (1.0 mmol), sodium azide (3.0 mmol), and alkynes (1.0 mmol) in a DMF:water mixture (8:2). Next, the Cu₂O microbeads were added into the reaction at a concentration of 20 mg/mL. The reaction mixture was

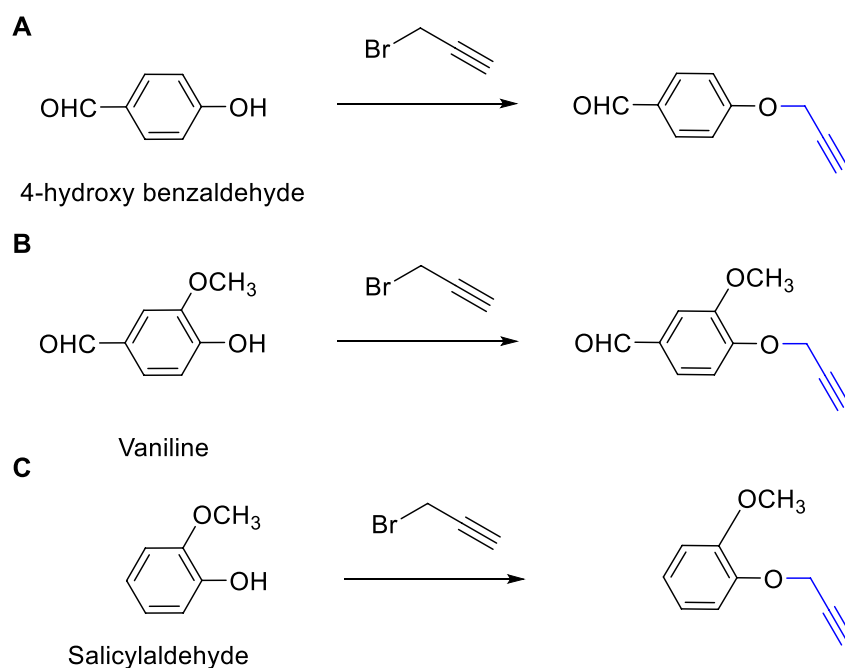


FIGURE 1
Synthesis of Alkynes Derivatives via the Reaction of Propargyl Bromide and Benzaldehyde Derivatives. **(A)** 4-(Prop-2-yn-1-yloxy) benzaldehyde, **(B)** 3-Methoxy-4-(prop-2-yn-1-yloxy) benzaldehyde, **(C)** 1-Methoxy-2-(prop-2-yn-1-yloxy) benzene. The reactions were conducted under vigorous stirring using K₂CO₃ as a catalyst, DMF as the solvent, with a reaction time of 2 h at a temperature of 80°C.

kept under vigorous stirring for duration of 3–4 h at a temperature of 90°C, and the progression of the reaction was monitored using the TLC. Upon the completion of the reaction, the addition of ice-cold water led to the precipitation of the product. The precipitate was subsequently filtered, washed with water, and subjected to recrystallization from ethanol to obtain 1,4-disubstituted 1,2,3-triazoles (Figures 2D–K). To assess the catalyst's reusability, it was recovered from the reaction mixture through centrifugation, followed by filtration and washing with acetone, chloroform, and hot ethanol. Subsequently, it was reused in the next three cycles after drying under the same reaction conditions.

2.4 Characterization

UV–vis spectrophotometer (UV-vis, SP-UV 500DB/VDB, Spectrum Instruments, Shanghai) was used to determine the light absorbance and bandgap energy of Cu₂O microbeads within the wavelength range of 220–600 nm. To assess the crystallinity and crystal structure of Cu₂O microbeads, X-ray diffraction (XRD, Miniflex 600 Rigaku, Tokyo, Japan) was performed with CuK α radiation (40 kV and 30 mA) at a wavelength of 1.5418 Å, utilizing a scanning speed of 0.5°. Chemical bonding in the Cu₂O microbeads were analyzed using Fourier transform infrared spectroscopy (FTIR, Spectrometer Agilent Cary, 630) covering a spectral range of 4,000–500 cm⁻¹. The particle size and morphology of Cu₂O microbeads were examined using scanning electron microscopy (SEM, Thermo Scientific, Quatro, Thermo Fisher

Scientific, Germany), and energy-dispersive X-ray (EDX) analysis was used to determine the elemental composition.

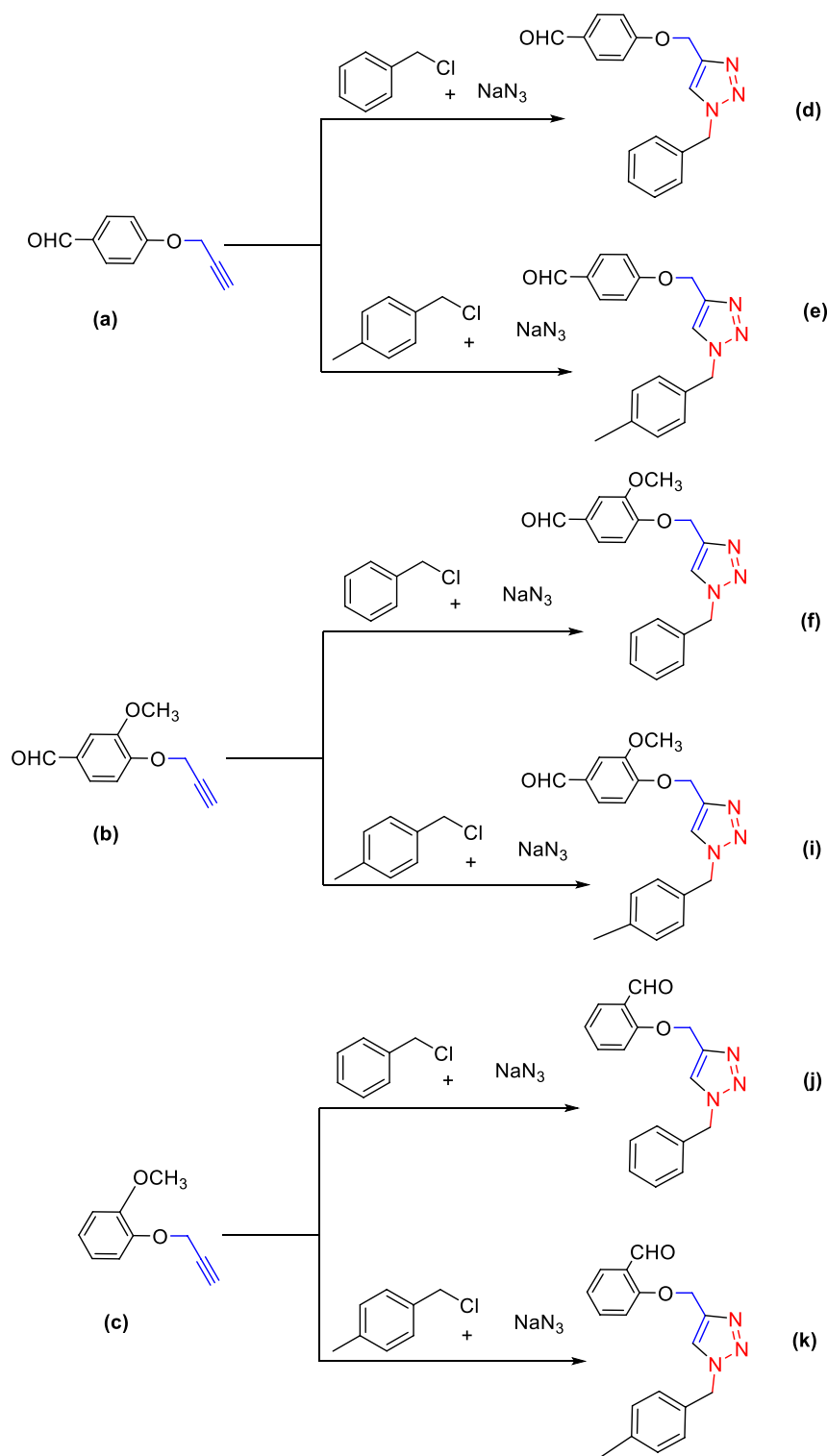
The synthesized alkynes (Figures 1A–C) and 1,4-disubstituted-1,2,3-triazole derivatives (Figures 2D–K) were confirmed through thin-layer chromatography (TLC, Silica Gel F254 Merck, Germany), assessment of melting points (System Kofler, LEICA VMHB, Germany), and Fourier-transform infrared spectroscopy (FTIR, FTIR spectrometer Agilent Cary 630, United States). Furthermore, ¹H and ¹³C nuclear magnetic resonance (NMR) spectra of the 1,4-disubstituted 1,2,3-triazoles were recorded on a (Bruker AV III spectrometer, France) at 300 MHz and 75 MHz, respectively. Chloroform was employed as the solvent, with tetramethyl silane (TMS) serving as an internal standard for NMR measurements.

3 Results and discussion

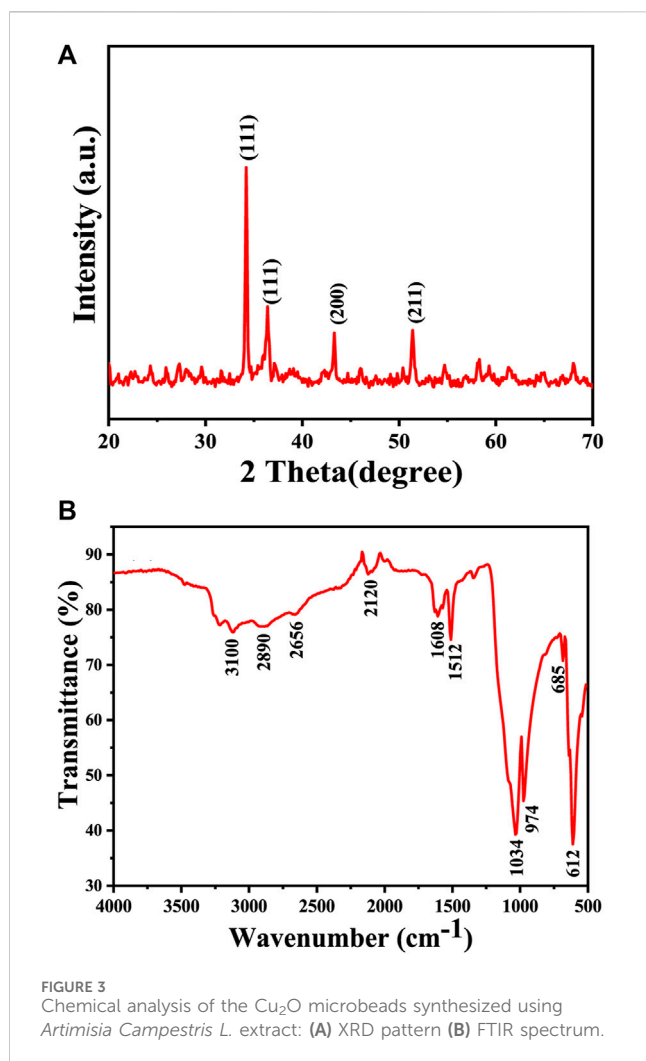
3.1 Characteristics of the Cu₂O microbeads

XRD, FTIR, and UV-Vis spectroscopy plays a crucial role in distinguishing between different copper oxide compounds, such as Cu₂O and CuO, by observing distinct patterns associated with their crystal structure and functional groups.

The XRD pattern of the Cu₂O microbeads sample is presented in Figure 3A. The XRD analysis results provided, with intense and sharp peaks at 34.21°, 36.50°, 43.28°, and 51.40° corresponding to the (111), (111), (200), and (211) planes, respectively, indicates the presence of the Cu₂O phase. These peaks are consistent with the

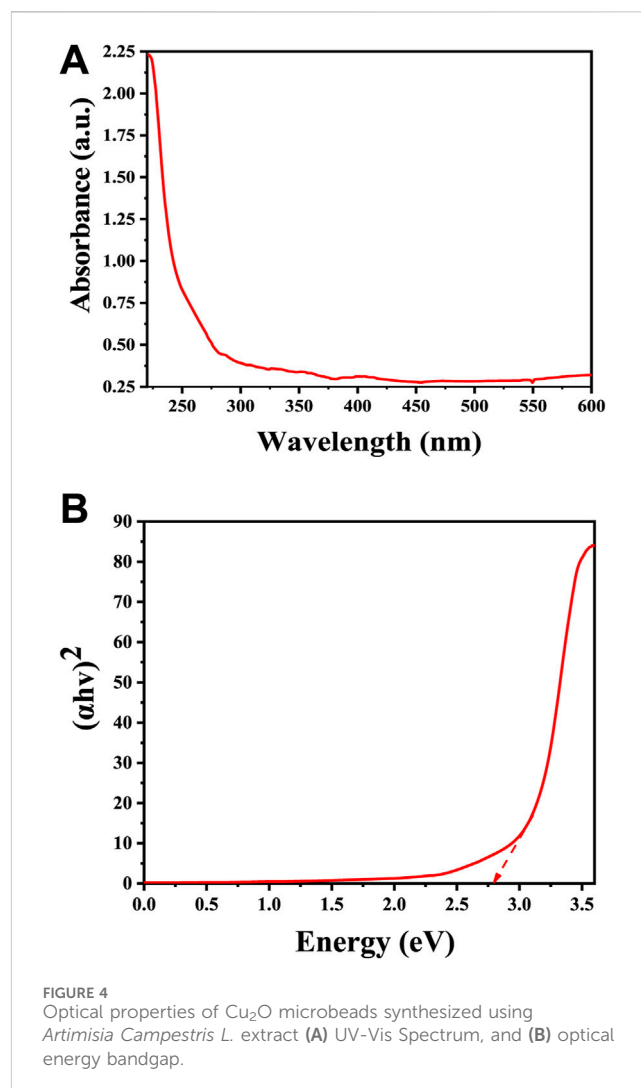
**FIGURE 2**

Synthesis of 1,4-Disubstituted 1,2,3-Triazoles from alkyne derivatives: **(A)** 4-(Prop-2-yn-1-yloxy) benzaldehyde, **(B)** 3-Methoxy-4-(prop-2-yn-1-yloxy) benzaldehyde, **(C)** 1-Methoxy-2-(prop-2-yn-1-yloxy) benzene with NaN_3 and benzyl chloride. The resulting 1,4-Disubstituted 1,2,3-Triazoles are represented by: **(D)** 4-((1-benzyl-1H-1,2,3-triazol-4-yl)methoxy)benzaldehyde, **(E)** 4-((1-(4-methylbenzyl)-1H-1,2,3-triazol-4-yl)methoxy)benzaldehyde, **(F)** 4-((1-benzyl-1H-1,2,3-triazol-4-yl)methoxy)-3-methoxybenzaldehyde, **(I)** 3-methoxy-4-((1-(4-methylbenzyl)-1H-1,2,3-triazol-4-yl)methoxy)benzaldehyde, **(J)** 2-((1-benzyl-1H-1,2,3-triazol-4-yl)methoxy)benzaldehyde, **(K)** 2-((1-(4-methylbenzyl)-1H-1,2,3-triazol-4-yl)methoxy)benzaldehyde. The chemical synthesis utilizes 20 mg/mL Cu_2O microbeads as a catalyst, a DMF: H_2O mixture as the solvent, with a reaction time of 3 h under reflux conditions at 90°C .



cubic close-packed (ccp) structure of Cu₂O (JCPDS, card no: 05–0667), no other phases like CuO are detected which indicating the purity of the prepared particles. The average crystallite size of the Cu₂O microbeads was calculated using the Debye-Scherrer formula ($D = K \lambda / \beta \cos \theta$), resulting in a size of 22.81 nm. Where, λ represents the X-ray wavelength (0.1541 nm), β is the full width half maximum (in radians), and θ is the diffraction angle.

FTIR spectrum in Figure 3B exhibits several characteristic peaks associated both the inorganic (Cu-O) elements and the phytochemicals within the extract. This indicates that the Cu₂O microbeads indeed incorporate phytochemicals, as results of the interactions occurring between the organic extract and copper ions throughout the synthesis process. The absorption peak at 610 cm⁻¹ corresponds to Cu-O stretching vibrations in the Cu₂O microbeads (Mannarmannan and Biswas, 2021), while the absorption peak at 3,100 cm⁻¹ attributed to O-H stretching vibrations. The reduced intensity of this O-H peak is linked to the oxidation of certain O-H groups during the reduction of Cu ions to Cu(I) (Lermontova et al., 2018). The broadened shape of the O-H peak may result from overlap with stretching vibrations of C-H bonds at 2,890 and 2,656 cm⁻¹, contributing to reduced intensity in the C-H group. This broadening might also come from interactions



between O-H groups in organic compounds from the organic extract and Cu⁺ ions, impacting the overall vibrational pattern (Maulana et al., 2022). The presence of atmospheric CO₂ during measurement is shown as peak at 2,120 cm⁻¹ associated with CO₂ stretching vibrations (Kumar et al., 2018). Furthermore, the peaks at 1,608 cm⁻¹ and 1,512 cm⁻¹ correspond to stretching vibrations of C=C and C=O bonds in the ketone (C=O) group, respectively (Maulana et al., 2022). The peak at 1,034 cm⁻¹ is attributed to the C-O stretching vibrations (Dou et al., 2021), and the bending modes of vibration for C-H bonds are indicated by the peak at 685 cm⁻¹.

UV-Vis spectra in Figure 4A shows a significant absorption peak at 220 nm, providing strong evidence for the successful formation of Cu₂O rather than CuO. This distinction is supported by previous studies, which note that Cu₂O and CuO phases exhibit unique absorption patterns in the UV-Vis spectrum due to differences in their electronic structures and bandgap energies. Specifically, CuO is characterized by a distinct absorption peak at around 640 nm, while Cu₂O displays a primary absorption peak within the 200–270 nm range, corresponding to a red shift in the visible spectrum (Bhardwaj et al., 2019). The bandgap of Cu₂O microbeads is typically around 2.7 eV (Figure 4B), which places it in the category of a direct bandgap semiconductor (Srinivasan et al., 2021). This further

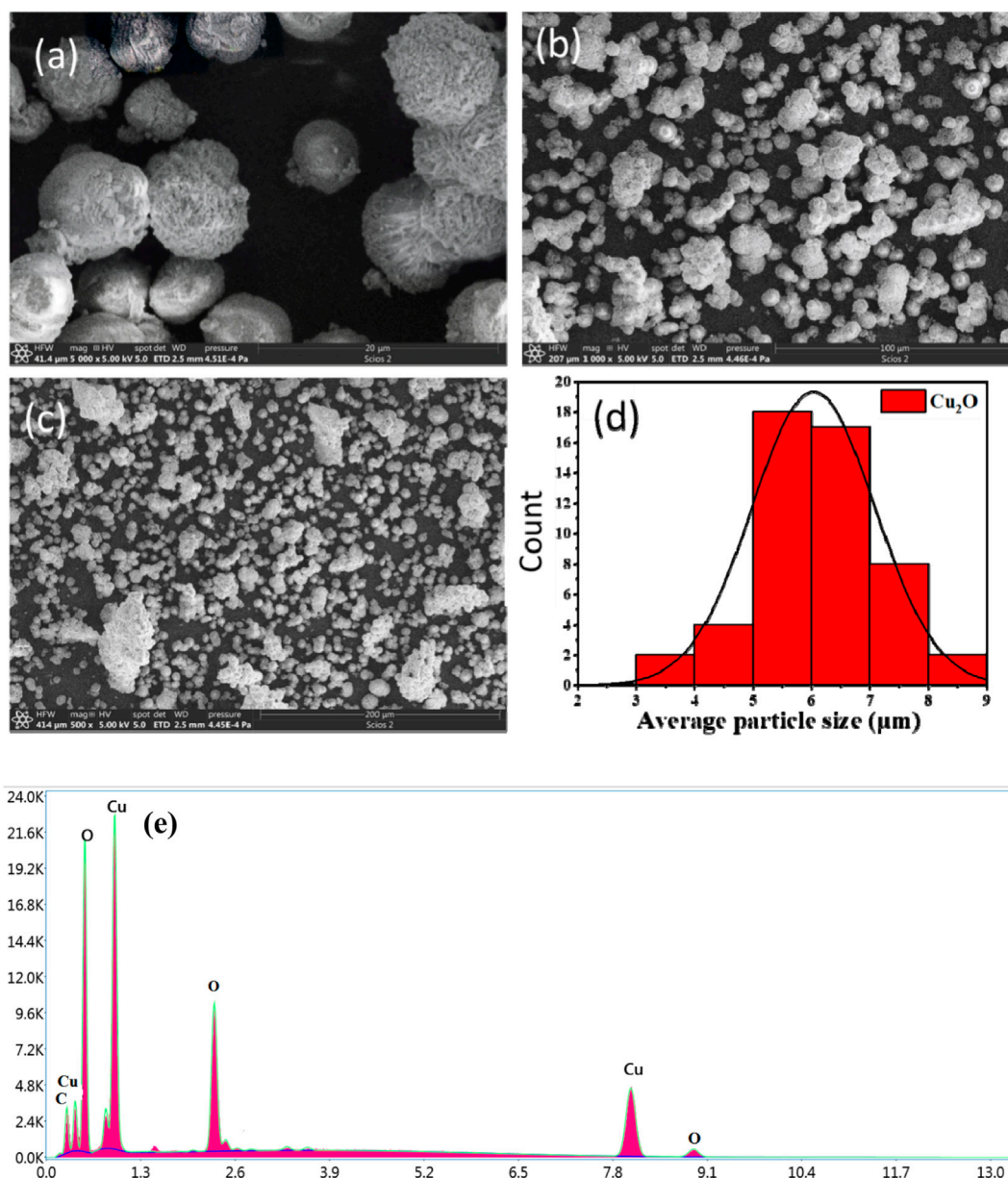


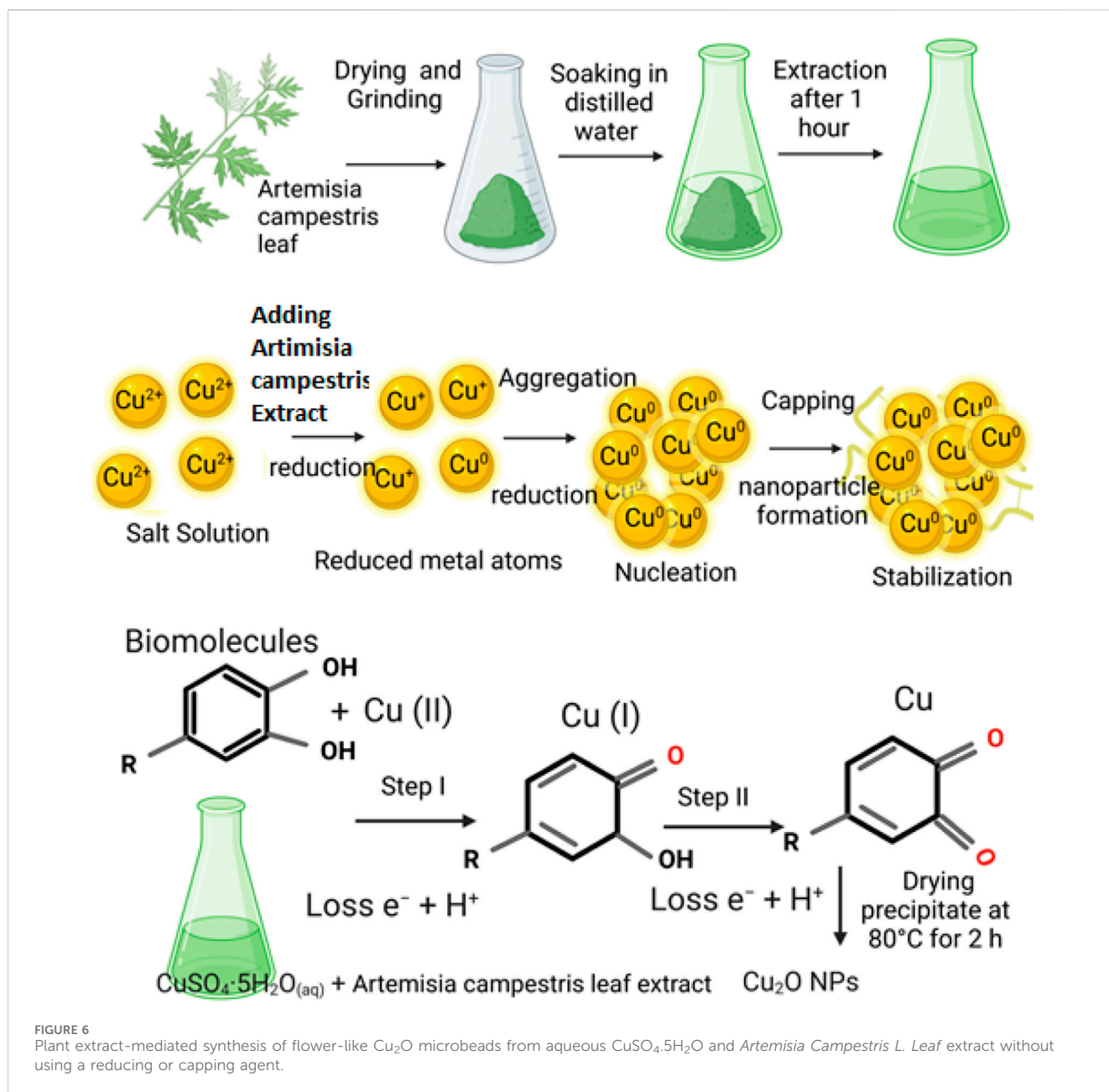
FIGURE 5 SEM analysis of Cu₂O microbeads synthesized using *Artemisia Campestris L.* extract (A–C) SEM images using different magnification, (D) histogram showing particle size distribution, and (E) EDX elemental analysis.

confirms that the prepared microbeads are Cu₂O and not CuO. The bandgap of CuO is smaller, typically around 1.3–1.7 eV (Jeong et al., 2022). The absorption and bandgap energy values can vary slightly based on factors such as crystal structure, size of the particles, and specific experimental conditions (Djamila et al., 2022).

Several factors exert a significant influence on the shape and particle size of Cu₂O microbeads, including solution pH, temperature, the quantity of plant extract utilized, and the concentrations of CuSO₄·5H₂O applied (Chokkareddy and Redhi, 2018). SEM images in Figure 5A–C clearly show spherical flower-like structures dominating the Cu₂O microbead morphology. The histogram in Figure 5D illustrates a uniform particle size distribution, indicating that the prepared Cu₂O microbeads fall

within the range of $6 \pm 3 \mu\text{m}$. To gain further insights into the elemental composition, energy dispersive X-ray spectroscopy (EDX) was employed. The SEM-EDX analysis in Figure 5E reveals a composition predominantly comprised of copper (Cu) at 54.91% and oxygen (O) at 23.73%, aligning with the expected elemental composition of Cu₂O phase. Notably, the presence of carbon (C) at 21.72% is observed, suggesting adsorption of the phytochemicals from the extract during the synthesis of the Cu₂O microbes (Pakzad et al., 2019). These findings align with the results obtained from FTIR analysis.

Formation of flower-like Cu₂O microbeads proposes a comprehensive three-stage growth process (Figure 6). This process undergoes multiple stages as follows: Initial Stage: The



process initiates with the formation of $\text{Cu}(\text{OH})_4^{2-}$ through a chemical reaction involving $\text{CuSO}_4 \cdot 5\text{H}_2\text{O}$ and an extract derived from *Artemisia Campestris L.* leaf. Intermediate Stage: Following the formation of $\text{Cu}(\text{OH})_4^{2-}$, a rapid reduction occurs with the support of bioactive molecules present in the *Artemisia Campestris L.* leaf extract. This reduction leads to the formation and growth of small Cu_2O nanoparticles, a dynamic event facilitated by continuous stirring. Second Stage: The small Cu_2O nanoparticles generated in the previous stage subsequently undergo a self-assembly or aggregation process, culminating in the formation of larger Cu_2O microbeads. This transformation from nanoparticles to microbeads signifies the second stage of growth. Final Stage: During the final stage, small building block nanoparticles within the Cu_2O microbeads undergo a transformation known as Ostwald ripening. This

process involves the enlargement of the Cu_2O nanoparticles over time. Here, it is important to note that the biomolecules derived from *Artemisia Campestris L.* leaf extract, which are absorbed on the nanoparticle surfaces, serve as structure-directing agents. These agents play a pivotal role in governing the surface state of the nanoparticles and led to formation of the flower-like Cu_2O microbeads.

3.2 Characterization of the synthesized products

The synthesized alkynes derivatives (Figures 1A–C) and 1,4-disubstituted-1,2,3-triazole derivatives (Figures 2D–K) were confirmed through TLC analysis, assessment of melting points,

TABLE 1 Characteristics of the alkynes and 1,4-disubstituted-1,2,3-triazole derivatives.

Alkynes					1,4-Disubstituted-1,2,3-triazole			
Derivatives	R ₁	R ₂	Melting (°C)	Yield (%)	Derivatives	R ₃	Melting (°C)	Yield ± 2.0 (%)
Figure 1A	CHO	H	81.0	83.0	Figure 2D	H	141	70.0
					Figure 2E	CH ₃	135	50.0
Figure 1B	CHO	OCH ₃	87.7	75.0	Figure 2F	H	125	85.3
					Figure 2I	CH ₃	110	33.0
Figure 1C	H	CHO	67.8	74.0	Figure 2J	H	139	70.0
					Figure 2K	CH ₃	142	68.0

TABLE 2 Effect of different reaction parameters on the synthesis of the 4-((1-benzyl-1H-1,2,3-triazol-4-yl)oxy)-3-methoxybenzaldehyde, reaction time of 3 h at 90°C.

Reactants	Solvent	Dose of Cu ₂ O catalyst	Products	Yield±2.0 (%)
3-Methoxy-4-(Prop-2-yn-1-yloxy)benzaldehyde (Figure 1B), NaN ₃ , and benzyl chloride	DMF: H ₂ O	1 mg/mL	4-((1-benzyl-1H-1,2,3-triazol-4-yl)oxy)-3-methoxybenzaldehyde (Figure 2F)	5.26%
	DMF: H ₂ O	5 mg/mL		15%
	DMF: H ₂ O	10 mg/mL		52%
	DMF: H ₂ O	15 mg/mL		57.9%
	DMF: H ₂ O	20 mg/mL		85.3%
	DMF: H ₂ O	30 mg/mL		70%
3-Methoxy-4-(Prop-2-yn-1-yloxy)benzaldehyde (Figure 1B), NaN ₃ , and benzyl chloride	EtOH: H ₂ O	20 mg/mL	4-((1-benzyl-1H-1,2,3-triazol-4-yl)oxy)-3-methoxybenzaldehyde (Figure 2F)	20%
	CHCl ₃	20 mg/mL		Non
	CH ₂ Cl ₂ : H ₂ O	20 mg/mL		30%
	Acetone	20 mg/mL		50%
	DMSO	20 mg/mL		56%

and FTIR spectroscopy (see [Supplementary Information](#)). [Table 1](#) list the melting points and the yield percentage of the alkynes and 1,4-disubstituted-1,2,3-triazole derivatives.

4-(Prop-2-yn-1-yloxy)benzaldehyde ([Figure 1A](#)): This compound appeared as light hazel crystals, yielding 83%. Its melting point was measured at 81°C. FTIR analysis (λ_{\max}) revealed characteristic peaks at 3,200, 2,110, 1,680, 1,600, 1,580, 1,160, 1,250, and 1000cm⁻¹ ([Supplementary Figure S2A](#)).

3-Methoxy-4-(Prop-2-yn-1-yloxy)benzaldehyde ([Figure 1B](#)): Light beige crystals were obtained with a 75% yield, and the compound exhibited a melting point of 87.7°C. FTIR (λ_{\max}) analysis displayed peaks at 3,220, 2,890, 2,110, 1,590, 1,700, 1,580, 1,250, 1,110, and 1,000 cm⁻¹ ([Supplementary Figure S2B](#)).

2-(Ethyloxy)benzaldehyde ([Figure 1C](#)): This compound was obtained as light beige crystals with a yield of 74%. Its melting point was measured at 67.8°C. FTIR analysis (λ_{\max}) indicated characteristic peaks at 3,280, 2,890, 2,110, 1,680, 1,600, 1,450, 1,280, 1,200, and 1000cm⁻¹ ([Supplementary Figure S2C](#)).

4-((1-Benzyl-1H-1,2,3-triazol-4-yl)oxy)benzaldehyde ([Figure 2D](#)): This compound was isolated in the form of light yellow crystals with a yield of 70%. It exhibited a melting point of 141 °C. FTIR analysis (λ_{\max})

revealed characteristic peaks at 2,100, 1,680, 1,600, 1,580, 1,250, 1,170, and 1000cm⁻¹. The ¹H NMR (300 MHz, Chloroform-d) spectrum displayed resonances at δ 9.57 (s, 1H), 7.57–7.47 (m, 2H), 7.13–7.02 (m, 3H), 7.04–6.92 (m, 2H), 6.83–6.72 (m, 2H), 5.24 (s, 2H), and 4.96 (d, 2H). The ¹³C NMR (75 MHz, Chloroform-d) exhibited peaks at δ 190.82, 163.15, 143.64, 134.33, 132.01, 130.37, 129.23, 128.94, 128.18, 122.87, 115.11, 62.20, and 54.35 ([Supplementary Figure S3](#)).

4-((1-(4-Methylbenzyl)-1H-1,2,3-triazol-4-yl)oxy)benzaldehyde ([Figure 2E](#)): Light yellow crystals were obtained with a yield of 50%, and the compound had a melting point of 135 °C. FTIR analysis (λ_{\max}) showed peaks at 2,100, 1,680, 1,600, 1,580, 1,250, 1,170, and 1000cm⁻¹. The ¹H NMR (300 MHz, Chloroform-d) spectrum revealed resonances at δ 9.61 (s, 1H), 7.61–7.50 (m, 2H), 6.91 (s, 4H), 6.86–6.76 (m, 2H), 5.22 (s, 2H), 4.98 (d, 2H), and 2.08 (s, 3H). The ¹³C NMR (75 MHz, Chloroform-d) exhibited peaks at δ 190.79, 163.18, 143.56, 138.93, 132.00, 131.28, 130.37, 129.88, 128.24, 122.72, 115.11, 62.22, 54.16, and 21.17 ([Supplementary Figure S4](#)).

4-((1-Benzyl-1H-1,2,3-triazol-4-yl)oxy)-3-methoxybenzaldehyde ([Figure 2F](#)): This compound appeared as yellow pale solid with an impressive yield of 85.3% and a melting point at 125 °C. FTIR analysis

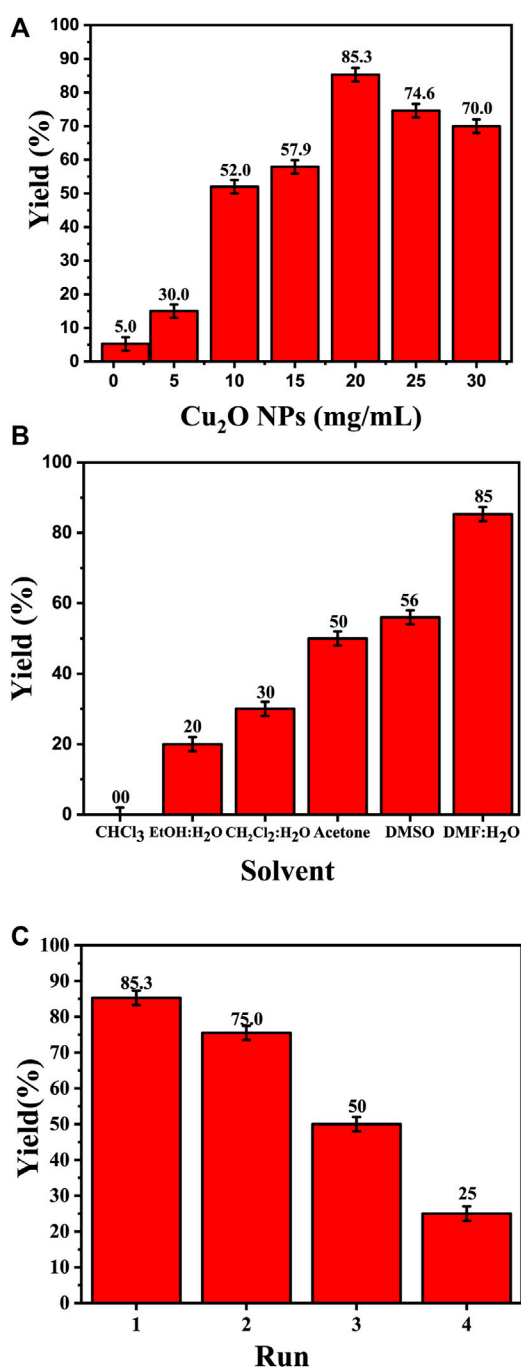


FIGURE 7
Effect of the catalyst on the synthesis of 4-((1-benzyl-1H-1,2,3-triazol-4-yl)oxy)-3-methoxybenzaldehyde. (A) Effect of the catalyst dose (Cu₂O microbeads mg/mL) in DMF:H₂O as solvent and 3 h reflux; (B) Effect of the type of solvent at Cu₂O microbeads catalyst dose of 20 mg/mL for 3 h reflux at 90°C; (C) Effect of catalyst reusability at Cu₂O microbeads catalyst dose of 20 mg/mL in DMF:H₂O as solvent and 3 h reflux at 90°C. All the synthesized products in these tests were confirmed by their melting points and TLC.

(λ_{\max}) displayed characteristic peaks at 2,100, 1,680, 1,580, 1,500, 1,250, 1,130, and 990 cm⁻¹. The ¹H NMR (400 MHz, Chloroform-d) spectrum revealed resonances at δ 9.90 (s, 1H), 7.64 (s, 1H), 7.51–7.39 (m, 5H), 7.32 (dd, 2H), 7.28 (s, 1H), 5.58 (s, 2H), 5.41 (s, 2H), 3.95 (s, 3H). The ¹³C NMR (75 MHz, Chloroform-d) spectrum featured

peaks at δ 190.88, 153.06, 149.99, 143.65, 134.31, 130.68, 129.18, 128.89, 128.18, 126.66, 123.08, 112.74, 109.33, 63.01, 56.00, and 54.32 (Supplementary Figure S5). RMN¹H (400 MHz, Chloroform-d).

4-((1-(4-Methylbenzyl)-1H-1,2,3-triazol-4-yl)oxy)-3-methoxybenzaldehyde (Figure 2I): The compound presented as yellow pale solid with a yield of 33%, and it had a melting point of 110°C. FTIR analysis (λ_{\max}) exhibited peaks at 2,100, 1,680, 1,580, 1,500, 1,260, 1,130, and 1,000 cm⁻¹. The ¹H NMR (400 MHz, Chloroform-d) revealed resonances at δ 89.84 (s, 1H), 7.55 (s, 1H), 7.45–7.37 (m, 2H), 7.21 (d, 1H), 7.17 (s, 4H), 5.47 (s, 2H), 5.34 (s, 2H), 3.89 (s, 3H), 2.35 (s, 3H). The ¹³C NMR (75 MHz, Chloroform-d) spectrum featured peaks at δ 190.89, 153.09, 149.99, 143.56, 138.88, 131.26, 130.66, 129.83, 128.24, 126.69, 122.97, 112.73, 109.30, 63.02, 56.01, 54.13, and 21.14 (Supplementary Figure S6).

2-((1-Benzyl-1H-1,2,3-Triazol-4-yl)oxy)benzaldehyde (Figure 2J): This compound was obtained in the form of white powder with a satisfactory yield of 70% and displayed a melting point at 139°C. FTIR analysis (λ_{\max}) revealed distinctive peaks at 2,100, 1,680, 1,600, 1,450, 1,260, and 1,050 cm⁻¹. In the ¹H NMR spectrum (300 MHz, Chloroform-d), resonances were observed at δ 10.41 (s, 1H), 7.81 (dd, 1H), 7.57–7.49 (m, 2H), 7.18 (s, 4H), 7.04 (tt, 1H), 5.49 (s, 2H), 5.29 (s, 2H), and 2.34 (s, 3H). The ¹³C NMR (75 MHz, Chloroform-d) spectrum featured peaks at δ 189.61, 160.48, 143.82, 136.01, 134.35, 129.24, 128.95, 128.71, 128.14, 125.13, 122.78, 121.37, 113.08, 62.64, and 54.36 (Supplementary Figure S7).

2-((1-(4-Methylbenzyl)-1H-1,2,3-Triazol-4-yl)oxy)benzaldehyde (Figure 2K): This compound was isolated as white powder with a yield of 68% and exhibited a melting point of 142°C. FTIR analysis (λ_{\max}) showed peaks at 2,100, 1,680, 1,600, 1,450, 1,250, and 1,050 cm⁻¹. In the ¹H NMR spectrum (300 MHz, Chloroform-d), resonances were observed at δ 10.41 (s, 1H), 7.81 (dd, 1H), 7.57–7.49 (m, 2H), 7.18 (s, 4H), 7.04 (tt, 1H), 5.49 (s, 2H), 5.29 (s, 2H), and 2.34 (s, 3H). The ¹³C NMR (75 MHz, Chloroform-d) spectrum featured peaks at δ 189.61, 160.51, 143.71, 138.91, 136.00, 131.30, 129.89, 128.65, 128.20, 125.12, 122.66, 121.33, 113.08, 62.65, 54.17, and 21.18 (Supplementary Figure S8).

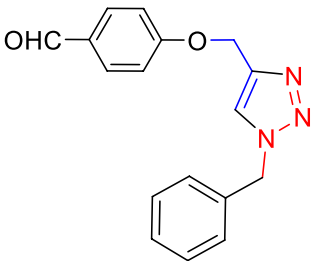
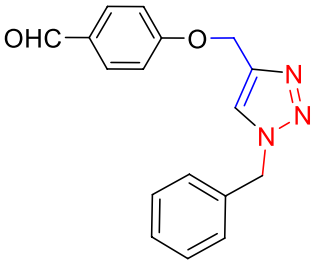
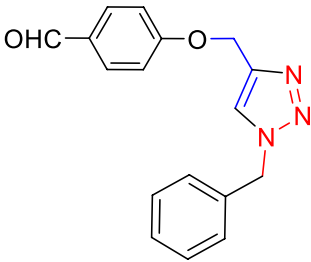
3.3 Optimizing the reaction parameters of organic synthesis

The composition of the reactants, including 3-Methoxy-4-(Prop-2-yn-1-yloxy)benzaldehyde, NaN₃, and benzyl chloride, significantly influences the synthesis of 4-((1-benzyl-1H-1,2,3-triazol-4-yl)oxy)-3-methoxybenzaldehyde. These reactants play a crucial role indicating the type and yield of the final product. Variations in reactant proportions or types could lead to altered reaction kinetics, impacting the formation of the desired product. This investigation focused on three key factors: initially, the tuning catalyst quantity, solvent selection, and subsequently, an assessment of the catalyst's reusability. Table 2 explores the optimal reaction conditions for synthesizing 4-((1-benzyl-1H-1,2,3-triazol-4-yl)oxy)-3-methoxybenzaldehyde (depicted in Figure 2F).

3.4 Effect of the amount of the catalyst

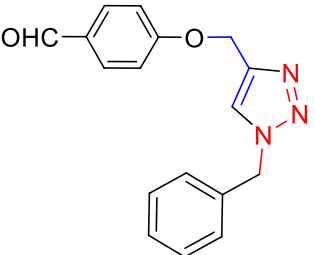
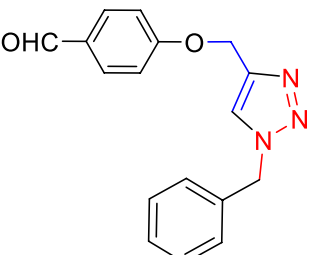
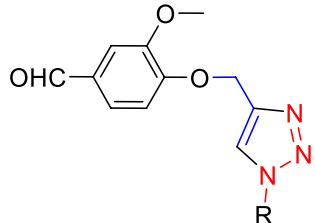
The amount of catalyst (measured in mg/mL) plays a key role in the synthesis of 4-((1-benzyl-1H-1,2,3-triazol-4-yl)oxy)-3-methoxybenzaldehyde (Figure 7A). The data presented in Table 2

TABLE 3 Synthesis of 4-((1-Benzyl-1H-1,2,3-triazol-4-yl)oxy)benzaldehyde and some derivatives in different reaction conditions from previous works (Figure 2D).

Reactant	Solvent	Condition	Catalyst	Product	Yield (%)	Ref
4-(Prop-2-yn-1-yloxy)benzaldehyde (Figure 1A), benzyl chloride, and sodium azide	EtOH/H ₂ O	15min microwave at 90°C	Cu(OAc).H ₂ O, 1,10-Phen.H ₂ O sodium ascorbate	 <p>Figure 2d</p>	82	González-Olvera et al. (2016)
				4-((1-Benzyl-1H-1,2,3-triazol-4-yl)oxy)benzaldehyde		
4-(Prop-2-yn-1-yloxy)benzaldehyde (Figure 1A), aryl azide	THF:H ₂ O	12h, room temperature	CuSO ₄ .5H ₂ O, sodium ascorbate	 <p>Figure 2d</p>	81.96	Kumar et al. (2013)
				4-((1-Benzyl-1H-1,2,3-triazol-4-yl)oxy)benzaldehyde		
aldehyde, benzyl azide	tert-butanol/water	20–24h, room temperature	CuSO ₄ .5H ₂ O, sodium ascorbate	 <p>Figure 2d</p>	92	Lermontova et al. (2018)
				4-((1-Benzyl-1H-1,2,3-triazol-4-yl)oxy)benzaldehyde		

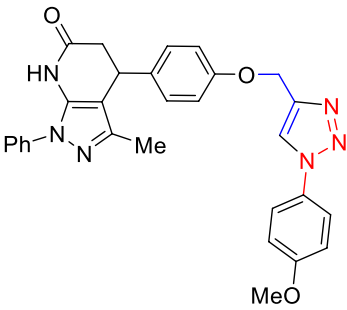
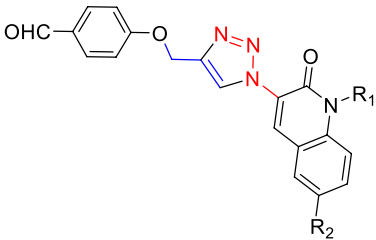
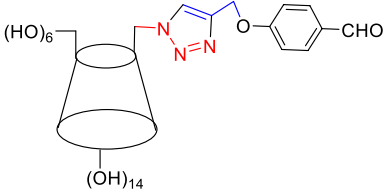
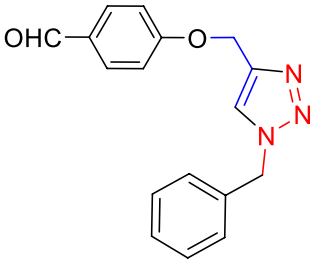
(Continued on following page)

TABLE 3 (Continued) Synthesis of 4-((1-Benzyl-1H-1,2,3-triazol-4-yl)oxy)benzaldehyde and some derivatives in different reaction conditions from previous works (Figure 2D).

Reactant	Solvent	Condition	Catalyst	Product	Yield (%)	Ref
4-(Prop-2-yn-1-yloxy)benzaldehyde (Figure 1A), benzyl aryl	Cu(OAc) ₂ · H ₂ O/H ₂ O	3h, room temperature	DHMC	 <p>Figure 2d</p>	87	Sharghi et al. (2014)
				4-((1-Benzyl-1H-1,2,3-triazol-4-yl)oxy)benzaldehyde		
4-(Prop-2-yn-1-yloxy)benzaldehyde (Figure 1A), sodium azide, benzyl bromide or methyl benzyl bromide	DMF/H ₂ O	4–16h, room temperature	CuSO ₄ ·5H ₂ O, sodium ascorbate	 <p>Figure 2d</p>	86	Lal et al. (2016)
				4-((1-Benzyl-1H-1,2,3-triazol-4-yl)oxy)benzaldehyde		
3-Methoxy-4-(Prop-2-yn-1-yloxy)benzaldehyde (Figure 1B), appropriate azide	DMF/H ₂ O	Overnight, stir, room temperature	CuSO ₄ ·5H ₂ O, sodium ascorbate	 <p>R=C₆H₅-CO-CH₂- R=4-Cl-C₆H₄-CO-CH₂- R=4-Br-C₆H₄-CO-CH₂- R=4-F-C₆H₄-CO-CH₂- R=5-CH₃-C₆H₄-CO-CH₂- R=4-HOOC-C₆H₄-</p>	36–49	Temraz et al. (2018)
				4-1H-1,2,3-triazol-4-yl)methoxy)-3-methoxybenzaldehyde derivatives		

(Continued on following page)

TABLE 3 (Continued) Synthesis of 4-((1-Benzyl-1H-1,2,3-triazol-4-yl)oxy)benzaldehyde and some derivatives in different reaction conditions from previous works (Figure 2D).

Reactant	Solvent	Condition	Catalyst	Product	Yield (%)	Ref
4-(Prop-2-yn-1-yloxy)benzaldehyde (Figure 1A), 3-methyl-1-phenyl-1H-pyrazol-5-amine, Meldrum's Acid, and 1-azido-4-methoxy benzene	EtOH	90 min, 100°C	PEG-400		82	Sindhu et al. (2016)
4-(Prop-2-yn-1-yloxy)benzaldehyde (Figure 1A), terminal alkynes, and 4-azido compounds	DMF/H ₂ O	12h, 30°C–50°C	CuSO ₄ ·5H ₂ O, sodium ascorbate		55–83	El-Sheref et al. (2019)
4-(Prop-2-yn-1-yloxy)benzaldehyde (Figure 1A)	DMF	15h, room temperature	CuSO ₄ ·5H ₂ O, sodium ascorbate		80	Wang et al. (2015)
4-(Prop-2-yn-1-yloxy)benzaldehyde (Figure 1A), benzyl chloride, and sodium azide	DMF:H ₂ O	3h, 90°C	Cu ₂ O microbeads 20 mg/mL	 <p style="text-align: center;">Figure 2d</p>	70.0	This work
				4-((1-Benzyl-1H-1,2,3-triazol-4-yl)oxy)benzaldehyde		

distinctly demonstrates the significant impact of the quantity of the Cu₂O catalyst on the final product yield. In the DMF: H₂O solvent system, the increase of the catalyst dosage from 1 mg/mL to 20 mg/mL, resulting in an increase in product yield: 5.26% ± 2.0%, 15% ± 2.0%, 52% ± 2.0%, 57.9% ± 2.0%, and reaching a maximum of 85.3% ± 2.0% at 20 mg/mL. However, with a further increase in the catalyst dosage to 25 and 30 mg/mL, the yield experienced a slight decrease to 74.6% ± 2.0% and 70% ± 2.0%, respectively. This indicates a clear correlation between the amount of catalyst and the yield of the product.

3.5 Effect of the type of solvent

The choice of solvent significantly influences the product yield in the synthesis of 4-((1-benzyl-1H-1,2,3-triazol-4-yl)oxy)-3-methoxybenzaldehyde (Figure 7B). The data in Table 2 indicates varied yields for different solvents, demonstrating the critical role of solvent selection in this chemical process. The DMF:H₂O system exhibited a direct correlation between the amount of catalyst (Cu₂O microbeads) and product yield, peaking at 85.3% ± 2.0% with 20 mg/mL of the Cu₂O microbeads. This combination proved most effective among the solvents tested. Conversely, other solvents, such as EtOH: H₂O, CHCl₃, CH₂Cl₂:H₂O, acetone, and DMSO, showed lower yields, ranging from 20% ± 2.0% to 56% ± 2.0% at the same Cu₂O microbeads dosage (20 mg/mL). The variance in yields underscores the significant impact of different solvents on reaction efficiency, affecting factors like solubility, reactivity, and stability of reactants and catalyst. The DMF: H₂O system stands out for enabling high yields, highlighting the critical role of solvent selection in optimizing the outcomes of this work.

3.6 Effect of the reusability of the Cu₂O microbeads

Figure 7C shows the effect of the reusability of the Cu₂O microbeads (initially at 20 mg/mL) on the yield of the organic product across multiple cycles. The initial yield in the first cycle is observed at 85.3% ± 2.0%. However, as the catalyst is reused in subsequent cycles, there is a notable decline in the yield. In the second cycle, the yield drops to 75% ± 2.0%, signifying a reduction from the initial yield despite the catalyst's reuse. This decreasing trend continues in the subsequent cycles, with yields of 50% in the third cycle and a further decrease to 25% ± 2.0% in the fourth cycle. The reduction in product yield over the four cycles indicates a decreasing catalyst efficiency, likely due to the loss of catalyst during the recovery process (centrifuging) and potential deactivation or alteration of the Cu₂O microbeads' surface through repeated use. This indicates the need for implementing strategies for catalyst recovery or regeneration to maintain consistent or improved yields in repeated usage.

3.7 Evaluation in the context of prior research

Plant-mediated synthesis of Cu₂O microbeads involves utilizing plant extracts as reducing and stabilizing agents (Figure 6). Bale et al. (Bale and Reddy, 2022) synthesized face-centered cubic (FCC) Cu₂O

nanoparticles using aqueous extracts of *Allium Cepa* and *Raphanus Sativus*, exhibiting average grain sizes ranging from 15 to 30 nm and 12–25 nm, respectively. In a similar vein, Chowdhury et al. (Chowdhury et al., 2021) used *Sechium edule extract* to synthesize Cu₂O nanoparticles with a face-centered cubic (fcc) lattice structure and an average crystallite size of 23.2 nm. Kumar et al. (Kumar et al., 2021) synthesized spherical and crystalline Cu₂O nanoparticles using *Andean Capuli Cherry*, with an average particle size of approximately 49 nm. Rai et al. (Rai and Chand, 2020) employed *rice* as a source of reducing and stabilizing agent to synthesize Cu₂O nanoparticles with homogeneous particle size of 9–10 nm. There is a scarcity of data regarding the synthesis of Cu₂O microbeads using *Artemisia Campestris L.* extract, emphasizing the unique contribution of our research. While previous research has showcased Cu₂O synthesis using plant extracts, the novelty of this work centers on the synthesis of flower-like Cu₂O microbeads, with unique morphology not reported before. This underscores the originality and potential innovation of this study in the realm of catalyst synthesis via plant-mediated methods.

The recyclability of Cu₂O microbeads stands out when compared to other catalysts in the synthesis of 4-((1-Benzyl-1H-1,2,3-triazol-4-yl)oxy) benzaldehyde (Table 3). Unlike traditional catalysts that may suffer decreased activity, Cu₂O microbeads provide an environmentally friendly and sustainable alternative with notable recyclability. In various reactions, including those using Cu(OAc).H₂O and CuSO₄.5H₂O, Cu₂O microbeads maintain a high yield (70.0%) even after multiple cycles. This underscores their efficiency and stability, making them an economically viable and environmentally friendly option. The recyclability of Cu₂O microbeads enhances organic synthesis efficiency, aligning with green chemistry principles by reducing waste and minimizing environmental impact. These characteristics emphasize the importance of Cu₂O microbeads as a sustainable catalyst in organic synthesis.

4 Conclusion

This study introduces an environmentally conscious approach to fabricate porous flower-like Cu₂O microbeads, serving as an eco-friendly alternative to conventional physicochemical synthesis methods. Leveraging the unique attributes of *Artemisia Campestris L. extract* as a dual reducing and stabilizing agent, the study achieved the production of flower-like Cu₂O microbeads characterized by exceptional catalytic properties. These biogenic porous flower-like Cu₂O microbeads demonstrated high efficiency as catalyst in the synthesis of 1,4-disubstituted 1,2,3-triazole derivatives through a one-pot, multi-component addition reaction. The outcomes underscore the remarkable capability of *Artemisia Campestris L. extract* to efficiently reduce, stabilize, and combine the primary formed Cu₂O particles, resulting in 6 μm microbeads exhibiting a flower-like morphology, an average crystallite size of 22.8 nm. These microbeads exhibit noteworthy catalytic activity, facilitating the synthesis of 1,4-disubstituted 1,2,3-triazole derivatives. Systematic investigations into key parameters, including catalyst quantity, solvent type, and catalyst reusability, revealed the catalyst's ability to enhance product's yield from 20% to 85.3%. This exceptional performance underscores the potential of

these Cu₂O microbeads for sustainable and efficient chemical transformations. This study plays a key role in moving towards a greener and more sustainable future. It contributes significantly to the field of catalysis and environmentally friendly materials, offering a promising direction for more eco-conscious chemical processes.

Data availability statement

The original contributions presented in the study are included in the article/[Supplementary Material](#), further inquiries can be directed to the corresponding authors.

Author contributions

HA: Data curation, Formal Analysis, Investigation, Methodology, Software, Validation, Visualization, Writing–original draft. AD: Conceptualization, Data curation, Formal Analysis, Investigation, Methodology, Software, Supervision, Validation, Writing–original draft. LS: Data curation, Formal Analysis, Investigation, Methodology, Writing–original draft, Validation. AS: Data curation, Formal Analysis, Investigation, Methodology, Validation, Writing–original draft. MO: Conceptualization, Data curation, Formal Analysis, Investigation, Methodology, Software, Validation, Writing–original draft. BD: Conceptualization, Data curation, Formal Analysis, Methodology, Software, Validation, Writing–original draft. ML: Data curation, Formal Analysis, Investigation, Methodology, Validation, Writing–original draft. MM: Data curation, Formal Analysis, Investigation, Software, Validation, Writing–original draft. IB: Data curation, Formal Analysis, Methodology, Software, Validation, Writing–original draft. ABe: Formal Analysis, Investigation, Methodology, Validation, Writing–original draft. AA: Formal Analysis, Resources, Validation, Visualization, Writing–review and editing, Funding acquisition. MB: Data curation, Formal Analysis, Funding acquisition, Validation, Writing–review and editing. ABa: Data

curation, Investigation, Methodology, Writing–original draft, Writing–review and editing, Conceptualization, Formal Analysis, Funding acquisition, Project administration, Resources, Software, Supervision, Validation, Visualization.

Funding

The author(s) declare financial support was received for the research, authorship, and/or publication of this article. ABa and AA express gratitude to the Egypt–France Joint Driver (Imhotep, Project No. 43990SF, 2020–2022) and the Researchers Supporting Project number (RSP-2024R78) at King Saud University, Riyadh, Saudi Arabia for their funding.

Conflict of interest

The authors declare that the research was conducted in the absence of any commercial or financial relationships that could be construed as a potential conflict of interest.

Publisher's note

All claims expressed in this article are solely those of the authors and do not necessarily represent those of their affiliated organizations, or those of the publisher, the editors and the reviewers. Any product that may be evaluated in this article, or claim that may be made by its manufacturer, is not guaranteed or endorsed by the publisher.

Supplementary material

The Supplementary Material for this article can be found online at: <https://www.frontiersin.org/articles/10.3389/fchem.2023.1342988/full#supplementary-material>

References

- Aronica, L. A., and Albano, G. (2022). Supported metal catalysts for the synthesis of N-heterocycles. *Catalysts* 12, 68. doi:10.3390/catal12010068
- Bale, V. K., and Reddy, K. H. (2022). Green synthesis, characterization and antimicrobial activity of nanosized Cuprous Oxide fabricated using aqueous extracts of *Allium cepa* and *Raphanus sativus*. *Int. J. Nano Dimens.* 13, 214–226. doi:10.22034/IJND.2022.687833
- Bhardwaj, A. K., Kumar, V., Pandey, V., Naraian, R., and Gopal, R. (2019). Bacterial killing efficacy of synthesized rod shaped cuprous oxide nanoparticles using laser ablation technique. *SN Appl. Sci.* 1, 1426–1428. doi:10.1007/s42452-019-1283-9
- Chokkareddy, R., and Redhi, G. G. (2018). "Green synthesis of metal nanoparticles and its reaction mechanisms," in *Green metal nanoparticles: synthesis, characterization and their applications* (United States: Wiley), 113–139.
- Choudhury, P., Chattopadhyay, S., De, G., and Basu, B. (2021). Ni-rGO–zeolite nanocomposite: an efficient heterogeneous catalyst for one-pot synthesis of triazoles in water. *Mater. Adv.* 2, 3042–3050. doi:10.1039/d1ma00143d
- Chowdhury, A., Peela, N. R., and Golder, A. K. (2021). Synthesis of Cu₂O NPs using bioanalytes present in *Secchium edule*: mechanistic insights and application in electrocatalytic CO₂ reduction to formate. *J. CO₂ Util.* 51, 101622. doi:10.1016/j.jcou.2021.101622
- Dai, J., Tian, S., Yang, X., and Liu, Z. (2022). Synthesis methods of 1, 2, 3-/1, 2, 4-triazoles: a review. *Front. Chem.* 10, 891484. doi:10.3389/fchem.2022.891484
- Daraie, M., Heravi, M. M., and Sarmasti, N. (2020). Synthesis of polymer-supported Zn (II) as a novel and green nanocatalyst for promoting click reactions and using design of experiment for optimization of reaction conditions. *J. Macromol. Sci. Part A* 57, 488–498. doi:10.1080/10601325.2020.1725389
- De Nino, A., Maiuolo, L., Costanzo, P., Algieri, V., Jiritano, A., Olivito, F., et al. (2021). Recent progress in catalytic synthesis of 1, 2, 3-triazoles. *Catalysts* 11, 1120. doi:10.3390/catal11091120
- De Nino, A., Merino, P., Algieri, V., Nardi, M., Di Gioia, M. L., Russo, B., et al. (2018). Synthesis of 1, 5-functionalized 1, 2, 3-triazoles using ionic liquid/iron (III) chloride as an efficient and reusable homogeneous catalyst. *Catalysts* 8, 364. doi:10.3390/catal8090364
- Djamila, B., Eddine, L. S., Abderrhmane, B., Nassiba, A., and Barhoum, A. (2022). *In vitro* antioxidant activities of copper mixed oxide (CuO/Cu₂O) nanoparticles produced from the leaves of *Phoenix dactylifera* L. *Biomass Conv. Bioref.* 1–14. doi:10.1007/s13399-022-02743-3
- Dou, L., Zhang, X., Zangeneh, M. M., and Zhang, Y. (2021). Efficient biogenesis of Cu₂O nanoparticles using extract of *Camellia sinensis* leaf: evaluation of catalytic, cytotoxicity, antioxidant, and anti-human ovarian cancer properties. *Bioorg. Chem.* 106, 104468. doi:10.1016/j.bioorg.2020.104468

- El-Sherief, E. M., Aly, A. A., Ameen, M. A., and Brown, A. B. (2019). Synthesis of new 4-(1, 2, 3-triazolo) quinolin-2 (1 H)-ones via Cu-catalyzed [3+ 2] cycloaddition. *Monatsh. für Chemie-Chemical Mon.* 150, 747–756. doi:10.1007/s00706-018-2342-4
- González-Olvera, R., Román-Rodríguez, V., Negrón-Silva, G. E., Espinoza-Vázquez, A., Rodríguez-Gómez, F. J., and Santillan, R. (2016). Multicomponent synthesis and evaluation of new 1, 2, 3-triazole derivatives of dihydropyrimidinones as acidic corrosion inhibitors for steel. *Molecules* 21, 250. doi:10.3390/molecules21020250
- Hui, H., Esmaili, E., Tayeb, R., He, Q., Abbaspour, S., Akram, M., et al. (2022). Biosynthesis, characterization, and application of Cu₂O nanoparticles originated from Cressa leaf extract as an efficient green catalyst in the synthesis of some chromenes. *J. Iran. Chem. Soc.* 19, 1261–1270. doi:10.1007/s13738-021-02378-7
- Jeong, D., Jo, W., Jeong, J., Kim, T., Han, S., Son, M.-K., et al. (2022). Characterization of Cu₂O/CuO heterostructure photocathode by tailoring CuO thickness for photoelectrochemical water splitting. *RSC Adv.* 12, 2632–2640. doi:10.1039/d1ra08863g
- Kawka, A., Hajdas, G., Kulaga, D., Koenig, H., Kowalczyk, I., and Pospieszny, T. (2023). Molecular structure, spectral and theoretical study of new type bile acid–sterol conjugates linked via 1, 2, 3-triazole ring. *J. Mol. Struct.* 1273, 134313. doi:10.1016/j.molstruc.2022.134313
- Kerour, A., Boudjadar, S., Bourzami, R., and Allouche, B. (2018). Eco-friendly synthesis of cuprous oxide (Cu₂O) nanoparticles and improvement of their solar photocatalytic activities. *J. Solid State Chem.* 263, 79–83. doi:10.1016/j.jssc.2018.04.010
- Kumar, B., Smita, K., Debut, A., and Cumbal, L. (2021). Green synthesis of cuprous oxide nanoparticles using Andean Capuli (Prunus serotina Ehrh. var. Capuli) cherry. *J. Clust. Sci.* 32, 1753–1760. doi:10.1007/s10876-020-01924-2
- Kumar, M., Das, R. R., Samal, M., and Yun, K. (2018). Highly stable functionalized cuprous oxide nanoparticles for photocatalytic degradation of methylene blue. *Mater. Chem. Phys.* 218, 272–278. doi:10.1016/j.matchemphys.2018.07.048
- Kumar, R., Arora, J., Prasad, A. K., Islam, N., and Verma, A. K. (2013). Synthesis and antimicrobial activity of pyrimidine chalcones. *Med. Chem. Res.* 22, 5624–5631. doi:10.1007/s00044-013-0555-y
- Lal, K., Yadav, P., and Kumar, A. (2016). Synthesis, characterization and antimicrobial activity of 4-((1-benzyl/phenyl-1 H-1, 2, 3-triazol-4-yl) methoxy) benzaldehyde analogues. *Med. Chem. Res.* 25, 644–652. doi:10.1007/s00044-016-1515-0
- Le, G. N. T., Cong, T. N., Van, T. P., Tuyet, M. N. T., Thi, L. N., Dang, C. H., et al. (2021). Green synthesis of cuprous oxide (Cu₂O) nano particles using aloe vera plant. *Vietnam J. Catal. Adsorpt.* 10, 54–58. doi:10.51316/jca.2021.028
- Lermontova, S., Grigoryev, I., Piskova, N., Balalaeva, I., Boyarskii, V., and Klapshina, L. (2018). Novel cyanoarylporphyrazines with triazole groups at the macrocycle periphery as potential sensitizers of photodynamic therapy and optical probes of intracellular viscosity. *Russ. J. General Chem.* 88, 2339–2346. doi:10.1134/s1070363218110154
- Librando, I. L., Mahmoud, A. G., Carabineiro, S. A., Guedes da Silva, M. F. C., Maldonado-Hódar, F. J., Geraldes, C. F., et al. (2021). Heterogeneous gold nanoparticle-based catalysts for the synthesis of click-derived triazoles via the azide-alkyne cycloaddition reaction. *Catalysts* 12, 45. doi:10.3390/catal12010045
- Mallik, M., Monia, S., Gupta, M., Ghosh, A., Toppo, M. P., and Roy, H. (2020). Synthesis and characterization of Cu₂O nanoparticles. *J. Alloys Compd.* 829, 154623. doi:10.1016/j.jallcom.2020.154623
- Mannarmannan, M., and Biswas, K. (2021). Phytochemical-assisted synthesis of cuprous oxide nanoparticles and their antimicrobial studies. *ChemistrySelect* 6, 3534–3539. doi:10.1002/slct.202004471
- Maulana, I., Fasya, D., Ginting, B., and Efendi, R. (2022). Biosynthesis of copper nanoparticles using methanol extract of sugar-apple leaves (Annonaceae squamosa), and its antioxidant activity. *J. Phys. Conf. Ser.* 2193, 012057. doi:10.1088/1742-6596/2193/1/012057
- Moeini-Eghbali, N., and Eshghi, H. (2023). Design and synthesis of nanorods Fe₃O₄@S-TiO₂/Cu as a green, and regioselective nanocatalyst in the synthesis of 1, 4-disubstituted-1, 2, 3-triazoles. *Inorg. Chem. Commun.* 156, 111181. doi:10.1016/j.inoche.2023.111181
- Murphin Kumar, P. S., Al-Muhtaseb, A. a. H., Kumar, G., Vinu, A., Cha, W., Villanueva Cab, J., et al. (2020). Piper longum extract-mediated green synthesis of porous Cu₂O: Mo microspheres and their superior performance as active anode material in lithium-ion batteries. *ACS Sustain. Chem. Eng.* 8, 14557–14567. doi:10.1021/acssuschemeng.0c05067
- Ojha, N. K., Zyryanov, G. V., Majee, A., Charushin, V. N., Chupakhin, O. N., and Santra, S. (2017). Copper nanoparticles as inexpensive and efficient catalyst: a valuable contribution in organic synthesis. *Coord. Chem. Rev.* 353, 1–57. doi:10.1016/j.ccr.2017.10.004
- Pakzad, K., Alinezhad, H., and Nasrollahzadeh, M. (2019). Green synthesis of Ni@Fe₃O₄ and CuO nanoparticles using Euphorbia maculata extract as photocatalysts for the degradation of organic pollutants under UV-irradiation. *Ceram. Int.* 45, 17173–17182. doi:10.1016/j.ceramint.2019.05.272
- Parvizi, J., Mahmoodi, N. O., Pirbasti, F. G., and Rassa, M. (2019). One pot multicomponent synthesis of novel bis-N-(1, 2, 3-triazolylacetyl) as potent antioxidant and antibacterial agents. *ChemistrySelect* 4, 5421–5426. doi:10.1002/slct.201900983
- Rai, R., and Chand, D. K. (2020). Multicomponent click reactions catalysed by copper (I) oxide nanoparticles (Cu₂O ONPs) derived using Oryza sativa. *J. Chem. Sci.* 132, 83–12. doi:10.1007/s12039-020-01774-5
- Roemer, M., Luck, I., and Proschogo, N. (2022). Cu (I) mediated azidation of halobenzenes, and Cu catalysed selective azide reduction to corresponding amines. *Adv. Synthesis Catal.* 364, 2957–2971. doi:10.1002/adsc.202200594
- Sasmal, A. K., Dutta, S., and Pal, T. (2016). A ternary Cu₂O–Cu–CuO nanocomposite: a catalyst with intriguing activity. *Dalton Trans.* 45, 3139–3150. doi:10.1039/c5dt03859f
- Shaabani, S., Tavousi Tabatabaei, A., and Shaabani, A. (2017). Copper (I) oxide nanoparticles supported on magnetic casein as a bio-supported and magnetically recoverable catalyst for aqueous click chemistry synthesis of 1, 4-disubstituted 1, 2, 3-triazoles. *Appl. Organomet. Chem.* 31, e3559. doi:10.1002/aoc.3559
- Sharghi, H., Shiri, P., and Aberi, M. (2014). An efficient catalytic system based on 7, 8-dihydroxy-4-methylcoumarin and copper (II) for the click synthesis of diverse 1, 4-disubstituted-1, 2, 3-triazoles under green conditions. *Mol. Divers.* 18, 559–575. doi:10.1007/s11030-014-9527-5
- Sharma, P., Rathod, J., Singh, A., Kumar, P., and Sasson, Y. (2018). Synthesis of heterogeneous Ru (ii)-1, 2, 3-triazole catalyst supported over SBA-15: application to the hydrogen transfer reaction and unusual highly selective 1, 4-disubstituted triazole formation via multicomponent click reaction. *Catal. Sci. Technol.* 8, 3246–3259. doi:10.1039/c7cy02619f
- Sindhu, J., Singh, H., Khurana, J., Bhardwaj, J. K., Saraf, P., and Sharma, C. (2016). Synthesis and biological evaluation of some functionalized 1 H-1, 2, 3-triazole tethered pyrazolo [3, 4-b] pyridin-6 (7 H)-ones as antimicrobial and apoptosis inducing agents. *Med. Chem. Res.* 25, 1813–1830. doi:10.1007/s00044-016-1604-0
- Srinivasan, S. S. G., Govardhanan, B., Ashok, M., and Kumar, M. S. (2021). Influence of deposition time on the visible-light-driven photocatalytic activity of Cu₂O thin films by reactive sputtering at room temperature. *Mater. Lett.* 284, 128980. doi:10.1016/j.matlet.2020.128980
- Sultana, J., and Sarma, D. (2020). Ag-catalyzed azide-alkyne cycloaddition: copper free approaches for synthesis of 1, 4-disubstituted 1, 2, 3-triazoles. *Catal. Rev.* 62, 96–117. doi:10.1080/01614940.2019.1673443
- Tehrani, M. B., Emani, P., Rezaei, Z., Khoshneviszadeh, M., Ebrahimi, M., Edraki, N., et al. (2019). Phthalimide-1, 2, 3-triazole hybrid compounds as tyrosinase inhibitors; synthesis, biological evaluation and molecular docking analysis. *J. Mol. Struct.* 1176, 86–93. doi:10.1016/j.molstruc.2018.08.033
- Temraz, M. G., Elzahhar, P. A., Bekhit, A. E.-D. A., Bekhit, A. A., Labib, H. F., and Belal, A. S. (2018). Anti-leishmanial click modifiable thiosemicarbazones: design, synthesis, biological evaluation and *in silico* studies. *Eur. J. Med. Chem.* 151, 585–600. doi:10.1016/j.ejmech.2018.04.003
- Torres-Arellano, S., Reyes-Vallejo, O., Enriquez, J. P., Aleman-Ramirez, J., Huerta-Flores, A., Moreira, J., et al. (2021). Biosynthesis of cuprous oxide using banana pulp waste extract as reducing agent. *Fuel* 285, 119152. doi:10.1016/j.fuel.2020.119152
- Varghese, R. J., Zikalala, N., and Oluwafemi, O. S. (2020). “Green synthesis protocol on metal oxide nanoparticles using plant extracts,” in *Colloidal metal oxide nanoparticles* (Amsterdam, Netherlands: Elsevier), 67–82.
- Varzi, Z., Esmaili, M. S., Taheri-Ledari, R., and Maleki, A. (2021). Facile synthesis of imidazoles by an efficient and eco-friendly heterogeneous catalytic system constructed of Fe₃O₄ and Cu₂O nanoparticles, and guarana as a natural basis. *Inorg. Chem. Commun.* 125, 108465. doi:10.1016/j.inoche.2021.108465
- Wang, Z., Guo, H., Yang, F., and Zhang, Y. (2015). The synthesis and dyes complexation properties of novel cyclodextrin derivatives with large conjugate acylhydrazone group. *J. Inclusion Phenom. Macrocycl. Chem.* 82, 101–108. doi:10.1007/s10847-015-0501-3
- Waris, A., Din, M., Ali, A., Ali, M., Afridi, S., Baset, A., et al. (2021). A comprehensive review of green synthesis of copper oxide nanoparticles and their diverse biomedical applications. *Inorg. Chem. Commun.* 123, 108369. doi:10.1016/j.inoche.2020.108369
- Wu, Z. G., Liao, X. J., Yuan, L., Wang, Y., Zheng, Y. X., Zuo, J. L., et al. (2020). Visible-light-mediated click chemistry for highly regioselective azide-alkyne cycloaddition by a photoredox electron-transfer strategy. *Chemistry–A Eur. J.* 26, 5694–5700. doi:10.1002/chem.202000252
- Yadav, S., Jain, A., and Malhotra, P. (2019). A review on the sustainable routes for the synthesis and applications of cuprous oxide nanoparticles and their nanocomposites. *Green Chem.* 21, 937–955. doi:10.1039/c8gc03303j